A mélange contribution to arc magmas recorded by Nd–Hf isotopic decoupling: An example from the southern Qiangtang Block, central Tibet

Peng Sun [a,b], Qiang Wang [a,b,c,*], Lu-Lu Hao [a,c,*], Wei Dan [a,c], Quan Ou [a], Zi-Qi Jiang [d], Gong-Jian Tang [a,c]

[a] State Key Laboratory of Isotope Geochemistry, Guangzhou Institute of Geochemistry, Chinese Academy of Sciences, Guangzhou 510640, China
[b] College of Earth and Planetary Sciences, University of Chinese Academy of Sciences, Beijing 100049, China
[c] CAS Center for Excellence in Deep Earth Science, Guangzhou 510640, China
[d] School of Earth Science, Guilin University of Technology, Guilin 541004, China

ARTICLE INFO

ABSTRACT

Subduction zones are the main sites of material exchange between the crust and mantle. Sediments subducted at these zones are widely considered to play a key role in generating arc magmas. Here we report whole-rock Nd–Hf isotopic compositions of late Mesozoic intermediate–felsic igneous rocks from the southern Qiangtang Block, central Tibet. The late Jurassic Rena Co (*ca.* 150 Ma) and Jiacuo (*ca.* 152 Ma) granodiorites, which were derived from ancient lower crust, show Nd–Hf isotopic coupling ($\Delta\varepsilon_{Hf}(t) = 0.7$–2.4). Conversely, the early Cretaceous Rena Co granodiorite porphyries (*ca.* 112 Ma), which were derived from juvenile lower crust, display marked Nd–Hf isotopic decoupling ($\Delta\varepsilon_{Hf}(t) = 7.5$). We suggest that the juvenile crust was compositionally andesitic and similar to the Duolong andesitic rocks (118–106 Ma) of the southern Qiangtang Block, which were derived by partial melting of the mélange (a physical mixture of mid-ocean ridge basalts, subducted sediments, and mantle-wedge peridotites). A simple mixing modeling indicates that the source of the early Cretaceous Duolong andesitic rocks includes 1–2% bulk subducted sediments. The Duolong andesitic rocks also show Nd–Hf isotopic decoupling ($\Delta\varepsilon_{Hf}(t) = 3.0$–11.3). Furthermore, the early Cretaceous Duolong dioritic and granitic rocks, which were generated by mixing between andesitic melts and ancient-lower-crust-derived magmas, display Nd–Hf isotopic decoupling. Thus, we infer a significant contribution of mélange melting in the Nd–Hf isotopic decoupling of early Cretaceous igneous rocks of the southern Qiangtang Block.

1. Introduction

Subduction zones are the principal sites of material exchange between crust and mantle (Zindler and Hart, 1986; Porter and White, 2009; Yogodzinski et al., 2010). Crustal materials are extracted from the mantle, and the mantle wedge is fertilized by subducted materials, such as altered oceanic crust and sediments. Arc magmas are the main products of oceanic subduction, and their geochemical compositions are strongly influenced by subducted components (Barry et al., 2006; Chauvel et al., 2009). Sediments are considered to readily enter the sub-arc mantle wedge during subduction (Plank and Langmuir, 1993, 1998; Hawkesworth et al., 1997; Plank, 2005), but the amount of sediment and the transport mechanisms are variable and remain uncertain. For example, some studies have argued that the mantle wedge is

metasomatized by fluids or melts released from the subducted slab (e.g., McCulloch and Gamble, 1991; Elliott et al., 1997). However, other studies have suggested that arc magmas can be generated by mélange melting (e.g., Castro et al., 2010, 2013; Marschall and Schumacher, 2012; Hao et al., 2016b; Nielsen and Marschall, 2017). In the former model, the subducted slab releases melts or fluids with fractionated trace-element signatures, which can metasomatize the mantle wedge to produce arc magmas. The latter model suggests that the slab–mantle interface is not a sharp plane. In this case, the strong geochemical gradient between crust and mantle rocks, together with shearing in combination with intense metasomatism, can generally trigger the formation of a transitional layer of mélange. The mélange is formed by the physical mixing of basaltic oceanic crust, subducted sediments, and mantle wedge peridotite along the slab–mantle interface. The mélange

can rise from the slab surface to the hot sub-arc mantle wedge, and partial melting of the mélange will form arc magmas with fractionated trace-element signatures (e.g., Marschall and Schumacher, 2012). The critical difference between the two models is the reversed order of mixing and trace-element fractionation, which will produce distinct isotopic signatures (Nielsen and Marschall, 2017).

The chemical and isotopic compositions of subducted sediments are different from those of the mantle (Plank and Langmuir, 1998; Chauvel et al., 2008; Yogodzinski et al., 2010). Mixing of components with different geochemical features may cause Nd–Hf isotopic decoupling. For instance, Nd–Hf isotopic decoupling in Cenozoic intra-oceanic arc volcanic rocks has been attributed to the subducted sediment components in their source (Marini et al., 2005; Chauvel et al., 2008, 2009; Yogodzinski et al., 2010; Nebel et al., 2011). Thus, it should be possible to use Nd–Hf isotopic decoupling to constrain the amount and transport mechanism of sediments introduced into the mantle wedge.

The southern margin of the southern Qiangtang Block (SQB) in central Tibet is considered to have been an Andean-type arc during the late Mesozoic (Zhang and Tang, 2009; Zhang et al., 2012, 2017; Li et al., 2014a; Hao et al., 2016a, b, 2019; Yang et al., 2019a, 2021; Liu et al., 2020). The SQB late Jurassic–early Cretaceous igneous rocks are thought to have formed during northward subduction of the Bangong–Nujiang oceanic lithosphere (Zhang and Tang, 2009; Zhang et al., 2012, 2017; Li et al., 2014a, b; Hao et al., 2016a, b; Yang et al., 2019a, 2021). In this paper, we report new whole-rock Nd–Hf isotope data for the SQB late Mesozoic igneous rocks. The results show that the Nd and Hf isotopic compositions are coupled and decoupled in the late Jurassic and early Cretaceous rocks, respectively. Combining the new results with previous data, we infer a substantial contribution of mélange melting to Nd–Hf isotopic decoupling of the SQB early Cretaceous igneous rocks. This study provides valuable insights into the causes of Nd–Hf isotopic decoupling and has important implications for tracing the amounts and mechanisms of sediment incorporation into the mantle wedge.
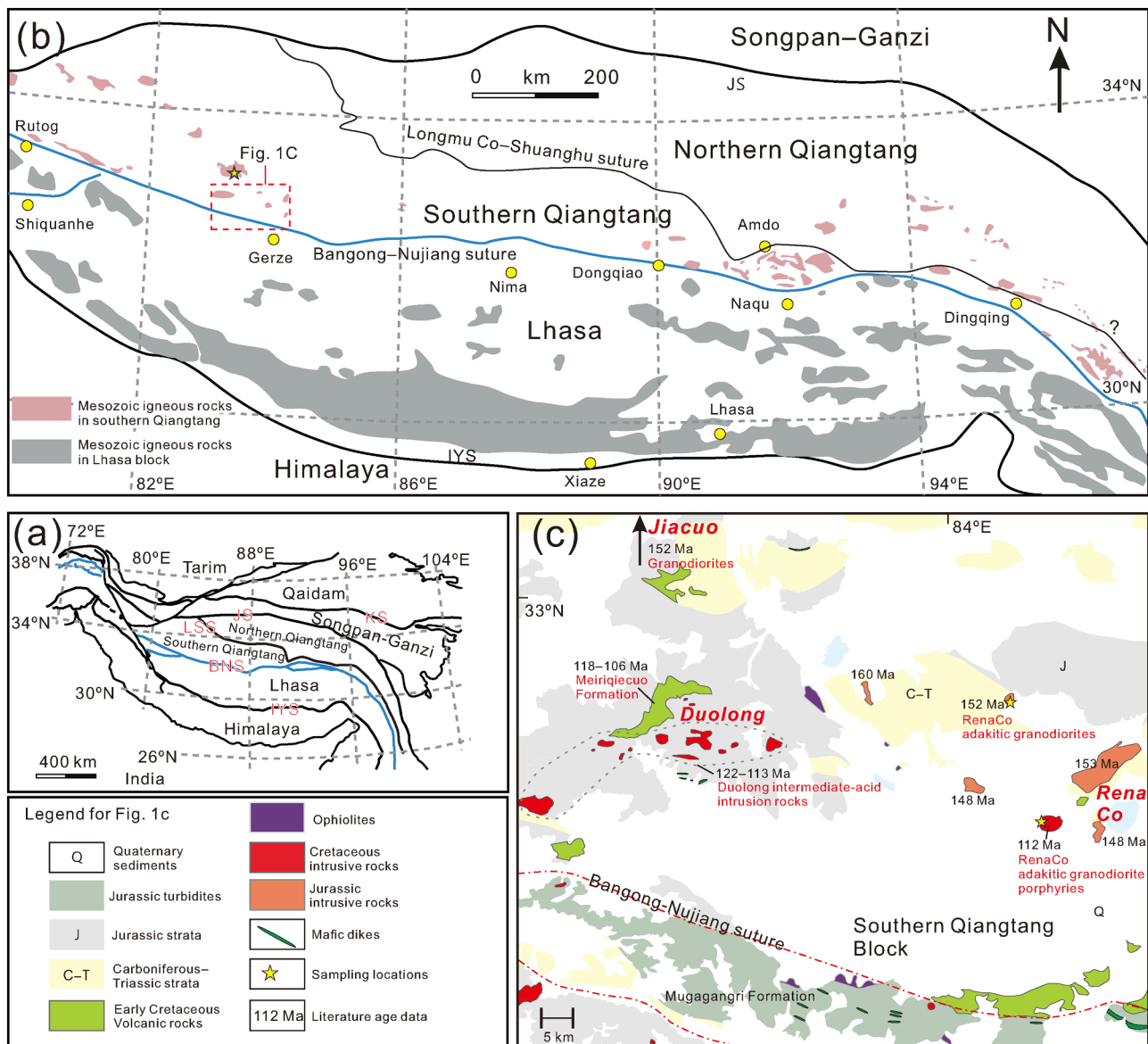
Fig. 1. (a) Tectonic framework of the Tibetan Plateau, modified after Yin and Harrison (2000), Chung et al. (2005), Zhang and Tang (2009), and Zhang et al. (2018). Main suture zones: Anyemaqen–Kunlun–Muztagh suture (AKMS); Jinsha suture (JS); Bangong–Nujiang suture (BNS); Indus–Yalu suture (IYS). (b) Map of the central Tibetan Plateau showing the distribution of Mesozoic igneous rocks of the SQB and Lhasa Block. (c) Simplified geological map showing the late Jurassic–early Cretaceous plutons and volcanic rocks of the SQB, central Tibet. Age data from the literature are from Li et al. (2013, 2014a, 2016b), Hao et al. (2016a, b), and Wu et al. (2016).

2. Geological setting and rock samples

The Tibetan Plateau comprises the Qaidam, Songpan–Ganzi–Hohxil, northern Qiangtang, southern Qiangtang, and Lhasa blocks. These blocks are separated from north to south by the Anyemaqen–Kunlun–Muztagh, Jinsha, Longmu Co–Shuanghu, and Bangong–Nujiang Suture Zones (Fig. 1a) (Chung et al., 2005; Zhang and Tang, 2009; Zhang et al., 2012). The Bangong–Nujiang Suture Zone (BNSZ) in the central Tibetan Plateau is a relic of the Bangong–Nujiang Tethyan Ocean (BNTO), which was located between the Lhasa Block and the SQB during the Mesozoic. The BSNZ extends for >2000 km from the Bangong Co area in the west to the Sanjiang area in the east (Fig. 1b) and comprises Jurassic–Cretaceous flysch, mélange, and ophiolitic fragments (Kapp et al., 2003; Zhang, 2004; Zhang et al., 2014). Strata of the SQB include Ordovician–Devonian metasedimentary rocks and sand-rich limestones, Carboniferous–Permian siliciclastic sedimentary and volcano-sedimentary rocks, Triassic limestones, and Jurassic sandstones and limestones (XZBGM, 1993).

The initiation of northward subduction of the BNTO slab beneath the SQB is thought to have occurred during the early Jurassic (*ca.* 195 Ma; Li et al., 2019 and references therein). However, the timing of closure of the BNTO remains debated. Previous studies have proposed several models involving oceanic subduction and collision settings to explain the petrogenesis of the SQB late Mesozoic igneous rocks: these rocks are variously thought to have formed during northward subduction of the BNTO slab (Zhang and Tang, 2009; Zhang et al., 2012, 2017; Li et al., 2014a, b; Hao et al., 2016a, b; Yang et al., 2019a, 2021) or during collision between the SQB and northern Lhasa block (Zhu et al., 2016; Wei et al., 2017). However, recent studies have suggested that the BNTO survived until the late early Cretaceous (*ca.* 100 Ma; Hao et al., 2019, Yang et al., 2019b, Cao et al., 2020).

The Jurassic igneous rocks of the SQB are widely distributed in the

Table 1
Geochronological data of the Late Mesozoic magmatic rocks in the southern Qiangtang Block.

Magmatic event	Region	Latitude	Longitude	Rock type	Age	Reference
Middle-Late Jurassic	Rutog			Biotite granite	168.1±0.9 Ma	Liu et al., 2014
Middle-Late Jurassic	Rutog			Biotite granite	168.4±0.9 Ma	Liu et al., 2014
Middle-Late Jurassic	Rutog			Quartz diorite	160.2±1.4 Ma	Li et al., 2014b
Middle-Late Jurassic	Rutog			Granodiorite	159.8±1.3 Ma	Li et al., 2014b
Middle-Late Jurassic	Rutog			Granodiorite	162.5±1.8 Ma	Li et al., 2014b
Middle-Late Jurassic	Rutog			Syenogranite	160.3±0.9 Ma	Li et al., 2014b
Middle-Late Jurassic	Jiacuo	33.566°N	83.933°E	Granodiorite	153.3±1.1 Ma	Sun et al., 2020
Middle-Late Jurassic	Jiacuo	33.583°N	83.400°E	Granodiorite	151.6±1.1 Ma	Sun et al., 2020
Middle-Late Jurassic	Duolong-RenaCo	32.910°N	83.850°E	Granodiorite	160.2±1.5 Ma	Wu et al., 2016
Middle-Late Jurassic	Duolong-RenaCo	32.904°N	83.850°E	Granite	159.5±1.2 Ma	Wu et al., 2016
Middle-Late Jurassic	Duolong-RenaCo	32.834°N	83.883°E	Diorite	156.1±1.2 Ma	Wu et al., 2016
Middle-Late Jurassic	Duolong-RenaCo	32.835°N	83.883°E	Granodiorite	164.6±2.9 Ma	Wu et al., 2016
Middle-Late Jurassic	Duolong-RenaCo	32.784°N	83.554°E	Granodiorite	168.9±1.7 Ma	Wu et al., 2016
Middle-Late Jurassic	Duolong-RenaCo	32.790°N	84.204°E	Diorite	153.0±1.9 Ma	Hao et al., 2016a
Middle-Late Jurassic	Duolong-RenaCo	32.777°N	84.199°E	Diorite	152.7±1.4 Ma	Hao et al., 2016a
Middle-Late Jurassic	Duolong-RenaCo	32.708°N	84.234°E	Diorite	148.4±2.5 Ma	Hao et al., 2016a
Middle-Late Jurassic	Duolong-RenaCo	32.889°N	84.084°E	Granodiorite	151.7±1.3 Ma	Hao et al., 2016a
Middle-Late Jurassic	Duolong-RenaCo	32.730°N	84.336°E	Dacite	154.3±0.6 Ma	Li et al., 2016c
Middle-Late Jurassic	Kangqiong	32.176°N	88.131°E	Granodiorite	149.9±2.1 Ma	Li et al., 2016d
Middle-Late Jurassic	Kangqiong	32.176°N	88.131°E	Granodiorite	147.6±2.4 Ma	Li et al., 2016d
Early Cretaceous	Qingcaoshan	33.227°N	83.191°E	Granodiorite	120.0±1.0 Ma	Li et al., 2014a
Early Cretaceous	Qingcaoshan	33.228°N	83.192°E	Diorite porphyry	119.0±1.0 Ma	Li et al., 2014a
Early Cretaceous	Qingcaoshan			Granodiorite	115.8±1.1 Ma	Li et al., 2017a
Early Cretaceous	Qingcaoshan			Granodiorite	118.9±0.9 Ma	Li et al., 2017a
Early Cretaceous	Qingcaoshan			Quartz diorite porphyry	116.4±1.0 Ma	Li et al., 2017a
Early Cretaceous	Qingcaoshan			Granite porphyry	112.7±0.5 Ma	Li et al., 2017a
Early Cretaceous	Qingcaoshan			Granodiorite	118.6±0.7 Ma	Li et al., 2017a
Early Cretaceous	Qingcaoshan			Porphyraceous granodiorite	118.8±0.7 Ma	Li et al., 2017a
Early Cretaceous	Qingcaoshan			Basalt	122.4±0.9 Ma	Fan et al., 2015
Early Cretaceous	Qingcaoshan			Dacite	120.4±0.5 Ma	Fan et al., 2015
Early Cretaceous	Duolong-RenaCo			Quartz diorite	126.4±0.6 Ma	Li et al., 2017b
Early Cretaceous	Duolong-RenaCo			Quartz diorite	122.1±0.7 Ma	Li et al., 2017b
Early Cretaceous	Duolong-RenaCo			Quartz diorite	124.6±0.6 Ma	Li et al., 2017b
Early Cretaceous	Duolong-RenaCo			Granodiorite	121.7±0.8 Ma	Li et al., 2017b
Early Cretaceous	Duolong-RenaCo			Diorite	120.5±1.2 Ma	Li et al., 2017b
Early Cretaceous	Duolong-RenaCo			Granodiorite porphyry	117.4±1.0 Ma	Li et al., 2013
Early Cretaceous	Duolong-RenaCo			Granodiorite porphyry	117.5±1.0 Ma	Li et al., 2013
Early Cretaceous	Duolong-RenaCo			Granodiorite porphyry	118.5±1.0 Ma	Li et al., 2013
Early Cretaceous	Duolong-RenaCo			Quartz diorite	118.4±1.1 Ma	Li et al., 2013
Early Cretaceous	Duolong-RenaCo			Quartz diorite	118.6±1.0 Ma	Li et al., 2013
Early Cretaceous	Duolong-RenaCo			Quartz diorite porphyry	113.0±1.9 Ma	Li et al., 2016b
Early Cretaceous	Duolong-RenaCo			Granodiorite porphyry	119.0±1.3 Ma	Li et al., 2016b
Early Cretaceous	Duolong-RenaCo			Granodiorite porphyry	116.6±1.3 Ma	Li et al., 2016b
Early Cretaceous	Duolong-RenaCo			Basaltic andesite	105.2±1.3 Ma	Li et al., 2016b
Early Cretaceous	Duolong-RenaCo			Basaltic andesite	110.2±0.7 Ma	Wei et al., 2017
Early Cretaceous	Duolong-RenaCo			Andesite	108.2±2.6 Ma	Wei et al., 2017
Early Cretaceous	Duolong-RenaCo			Andesite	110.5±1.2 Ma	Wei et al., 2017
Early Cretaceous	Duolong-RenaCo			Andesite	113.0±2.1 Ma	Wei et al., 2017
Early Cretaceous	Duolong-RenaCo			Rhyolite	109.3±2.2 Ma	Wei et al., 2017
Early Cretaceous	Duolong-RenaCo	32.877°N	83.506°E	Andesite	110.1±0.7 Ma	Wang et al.,2015
Early Cretaceous	Duolong-RenaCo	32.723°N	84.173°E	Granodiorite	111.7±0.9 Ma	Hao et al., 2016a
Early Cretaceous	Gerze–Bizha			Diorite	122.2±1.8 Ma	Hao et al., 2016b
Early Cretaceous	Gerze–Bizha			Basalts	107.7±1.9 Ma	Hao et al., 2019
Early Cretaceous	Gerze–Bizha			Dacite	105.6±1.2 Ma	Hao et al., 2019

Rutog, Qingcaoshan–Jiacuo, Duolong–Rena Co, and Kangqiong areas and are composed of 169–148 Ma intermediate–felsic intrusive rocks and minor extrusive rocks (Li et al., 2014b, c, d; Liu et al., 2014; Hao et al., 2016b; Wu et al., 2016; Sun et al., 2020). The early Cretaceous igneous rocks of the SQB are distributed locally in the Qingcaoshan, Duolong–Rena Co, and Gerze–Bizha areas and are composed mainly of 126–105 Ma intermediate–felsic intrusive rocks and andesitic volcanic rocks with minor basalt, dacite, and rhyolite (Li et al., 2013, 2014a, 2016b, 2017a, b; Fan et al., 2015; Wang et al., 2015; Hao et al., 2016a, b, 2019; Wei et al., 2017). Geochronological data for the SQB late Mesozoic magmatic rocks are listed in Table 1.

Our two study areas are located near Jiacuo and Rena Co (Fig. 1b, c). Granodiorite plutons and dikes (153–152 Ma) in the Jiacuo area are intruded into upper Carboniferous slate and lower Permian sandstone. The granodiorites are composed mainly of plagioclase (30–50 vol%), K-feldspar (~10 vol%), quartz (20–25 vol%), and minor biotite and amphibole (for specific mineral proportions, refer to Sun et al., 2020). Adakitic granodiorites (152–148 Ma) and granodiorite porphyries (112 Ma) in the Rena Co area are intruded into lower Carboniferous slate. The adakitic granodiorites are composed predominantly of plagioclase (60–65 vol%), quartz (10–15 vol%), and biotite (10–15 vol%). Granodiorite porphyries are typically porphyritic and composed of 40–50 vol% phenocrysts of plagioclase, biotite, and quartz, together with a groundmass of K-feldspar and quartz (for specific mineral proportions, refer to Hao et al., 2016a).

3. Analytical methods

Whole-rock Hf isotope analyses were performed at the State Key Laboratory of Isotope Geochemistry, Guangzhou Institute of Geochemistry, Chinese Academy of Sciences (SKLaBIG, GIGCAS), Guangzhou, China. The least altered samples were selected for Hf isotopic analysis. Surfaces of the samples were removed with a rock slicer, and the samples were crushed manually into small chips of 0.5–1.0 cm in size, powdered to ~200 mesh in an agate mortar, rinsed with distilled water, and cleaned three times in an ultrasonic bath. About 100 mg of sample powder was mixed with 200 mg of $Li_2B_4O_7$, placed in a platinum crucible, and melted in a Rigaku high-frequency fusion apparatus at 1200 °C. The melt was cooled rapidly to form glasses that were dissolved in 2 M HCl. Hf was separated from the matrix and interfering elements by HCl-single-column Ln-Spec extraction chromatography. The Hf isotopic compositions of the selected samples were determined using a Micromass Isoprobe multicollector–inductively coupled plasma–mass spectrometry (MC–ICP–MS) system. The detailed analytical procedures are described in Li et al. (2006). The measured $^{176}Hf/^{177}Hf$ ratios were normalized to $^{176}Hf/^{177}Hf = 0.7325$, and the measured $^{176}Hf/^{177}Hf$ ratio of the BHVO-2 standard, determined during analysis of the

unknowns, was 0.283079 ± 0.000004 (2σ; n = 2). Whole-rock Hf isotopic data, along with whole-rock major- and trace-elemental and Sr–Nd isotopic and zircon Hf isotopic data, for the late Jurassic–early Cretaceous igneous rocks in the Qingcaoshan–Jiacuo and Duolong–Rena Co areas of the SQB are given in Supplementary Table 1.

4. Results

4.1. Late Jurassic igneous rocks

The Jiacuo granodiorites (153–152 Ma; Sun et al., 2020) have moderate SiO_2 (64.8–68.4 wt%; Fig. 2a) and low MgO (1.6–2.3 wt%) and Mg# (47–49) [Mg# = Mg/(Mg + Fe)]. They have high K_2O contents (4.2–5.2 wt%) and belong to the high-K calc-alkaline series (Fig. 2b). Almost all of the samples exhibit enrichment in light rare earth elements (LREEs), depletion in high-field-strength elements (HFSEs; e.g., Nb, Ta, and Ti; Fig. 3a, b), and slight negative Eu anomalies (Eu/Eu* = $Eu_N/\sqrt{Sm_N \times Gd_N}$ = 0.77–0.80). They show uniform initial $^{87}Sr/^{86}Sr$ ratios of 0.7101–0.7102 and $\varepsilon_{Nd}(t)$ values of −7.7 to −7.6 (Fig. 5b), similar to those of ancient-lower-crust-derived magmatic rocks in the SQB (Hao et al., 2016a). The Jiacuo granodiorites show whole-rock $\varepsilon_{Hf}(t)$ values of −9.8 to −9.5 and lie on the terrestrial array in a $\varepsilon_{Nd}(t)$–$\varepsilon_{Hf}(t)$ diagram (Fig. 5a).

Compared with the Jiacuo granodiorites, the Rena Co adakitic granodiorites (152–148 Ma) have similar SiO_2 (63.3–66.2 wt%; Fig. 2a), MgO (1.0–1.6 wt%), and Mg# (33–42) but higher Sr (610–654 ppm) and lower heavy REEs (HREEs; Fig. 3a, b), such as Yb of 0.3–0.6 ppm and Y of 6.9–8.8 ppm. They exhibit high $(La/Yb)_N$ (23–96) and Sr/Y (51–137) ratios and are therefore classified as adakites (Defant and Drummond, 1990). The Rena Co adakitic granodiorites show negligible Eu anomalies (Eu/Eu* = 0.92–1.03) and are characterized by arc-like geochemical signatures, such as enrichment in large-ion lithophile elements (LILEs) and negative Nb and Ta anomalies. The whole-rock Sr–Nd isotopic compositions of the Rena Co adakitic granodiorites ($^{87}Sr/^{86}Sr(i)$ = 0.7069–0.7086, $\varepsilon_{Nd}(t)$ = −7.6 to −3.7) are similar to those of the Jiacuo granodiorites (Fig. 5b). In addition, the Rena Co samples display whole-rock $\varepsilon_{Hf}(t)$ values of −2.6 (Fig. 5a). Their Nd–Hf isotopic compositions are close to the terrestrial array (Fig. 5a).

4.2. Early Cretaceous igneous rocks

The Duolong andesitic rocks (118–106 Ma; Li et al., 2016b; Wang et al., 2015; Wei et al., 2017; Zhang et al., 2017) consist mainly of andesites and basaltic andesites with minor basalts. They show variable SiO_2 (49.4–61.8 wt%; Fig. 2a), MgO (0.5–6.6 wt%), and Mg# (16–59), which may indicate their complex sources and/or evolution processes.
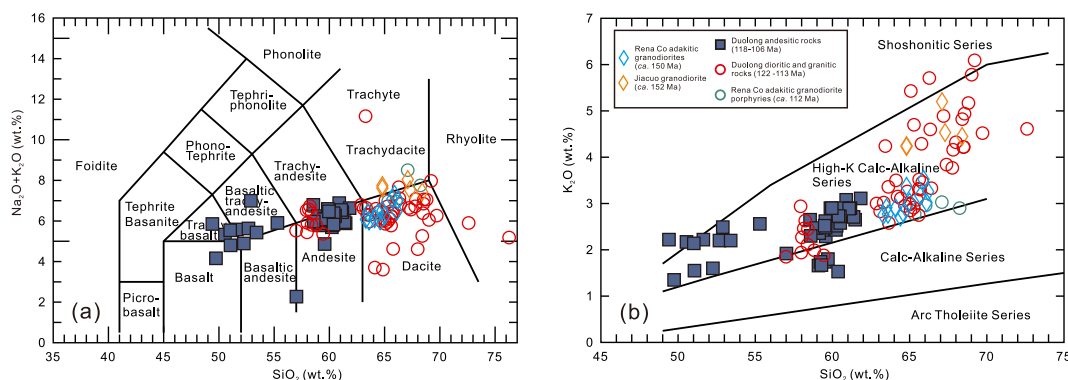
Fig. 2. (a) Total-alkali–silica classification diagram (Middlemost, 1994). (b) K_2O–SiO_2 diagram (Peccerillo and Taylor, 1976). Data for the Jurassic Jiacuo granodiorites and Rena Co adakitic granodiorites are from Sun et al. (2020) and Hao et al. (2016a), respectively; for the Cretaceous Duolong andesitic rocks are from Li et al. (2016b), Wang et al. (2015), and Wei et al. (2017); for the Cretaceous Duolong dioritic and granitic rocks are from Li et al. (2013, 2016b) and Zhu et al. (2015a, b); and for the Cretaceous Rena Co adakitic granodiorite porphyries are from Hao et al. (2016a).
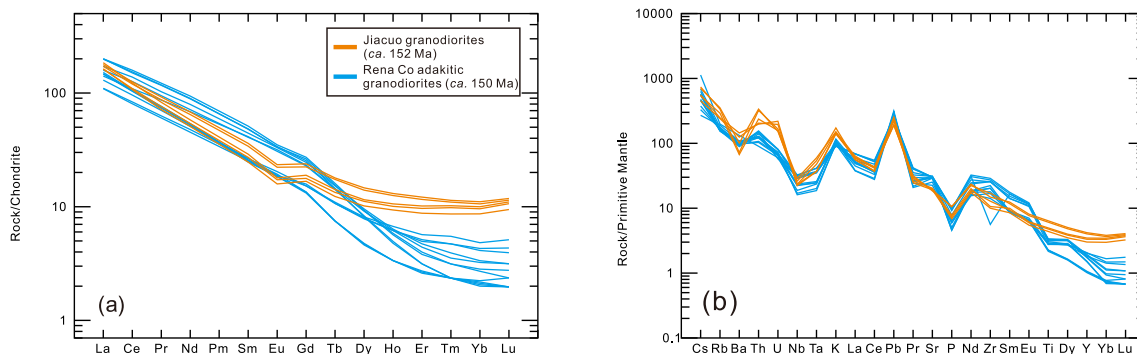
Fig. 3. (a) Chondrite-normalized REE pattern diagram and (b) primitive-mantle-normalized trace-element variation diagram for the SQB late Jurassic igneous rocks. Data sources are the same as Fig. 2. Chondrite and primitive-mantle normalization values are from Sun and McDonough (1989).

These rocks have K_2O contents of 1.4–3.1 wt% and plot in the high-K calc-alkaline series, with a few samples belonging to the calc-alkaline series (Fig. 2b). They display parallel REE and trace-element distribution patterns (Fig. 4a, b), with slight negative Eu anomalies (Eu/Eu* = 0.80–0.94), and have total REE contents of 122–205 ppm. The Duolong andesitic rocks show more depleted whole-rock Sr–Nd and zircon Hf isotopic compositions ($^{87}Sr/^{86}Sr(i)$ = 0.7045–0.7071, $\varepsilon_{Nd}(t)$ = −1.8 to +3.6, $\varepsilon_{Hf}(t)$ = +1.3 to +12.9) relative to the Jurassic magmatic rocks of the SQB (Fig. 5a, b). Notably, their Nd–Hf isotopic compositions lie away from the terrestrial array (Fig. 5a), with $\Delta\varepsilon_{Hf}(t)$ = 3.0–11.3 (Vervoot et al., 2011; $\Delta\varepsilon_{Hf}(t)$ = $\varepsilon_{Hf}(t)$ − 1.55 × $\varepsilon_{Nd}(t)$ − 1.21).

The Duolong diorites and granites (122–113 Ma; Li et al., 2011, 2013, 2014a, 2016a, 2017a, b) have variable SiO_2 (57.0–72.6 wt%; Fig. 2a), K_2O (1.9–10.1 wt%), MgO (0.4–3.9 wt%), and Mg# (27–59) and plot within the high-K calc-alkaline field (Fig. 2b). They are enriched in LILEs and depleted in HFSEs and have slight negative to positive Eu anomalies (Eu/Eu* = 0.73–1.50; Fig. 4a, b). In addition, they exhibit lower total REE contents (50–139 ppm) compared with the Duolong andesitic rocks. Their whole-rock Sr–Nd isotopic compositions vary over a wide range, with $^{87}Sr/^{86}Sr(i)$ = 0.7051–0.7078 and $\varepsilon_{Nd}(t)$ = −6.2 to +3.3, and plot between those of the Duolong andesitic rocks and Jiacuo/Rena Co granodiorites (Fig. 5b). The Duolong diorites and granites show relatively homogeneous and depleted zircon Hf isotopic compositions ($\varepsilon_{Hf}(t)$ = +4.5 to +6.8; Fig. 5a) compared with the variable Nd isotopic compositions. Thus, they plot above the terrestrial array, with $\Delta\varepsilon_{Hf}(t)$ = 6.3–12.3 (Fig. 5a).

The Rena Co adakitic granodiorite porphyries (112 Ma; Hao et al., 2016a) show slightly higher SiO_2 (67.2–69.7 wt%; Fig. 2a) and lower MgO (0.4–1.6 wt%) and Mg# (15–42) compared with the Duolong andesitic rocks and diorites–granites. They exhibit arc-like trace-element patterns with enrichment in LILEs and depletion in HFSEs. They are characterized by low Y (8.2–8.6 ppm) and Yb (0.9–1.0 ppm) and high Sr (438–502 ppm), $(La/Yb)_N$ (16–20), and Sr/Y (51–61), belonging

to adakites (Defant and Drummond, 1990). The Rena Co adakitic granodiorite porphyries are characterized by depleted whole-rock Sr–Nd–Hf isotopic compositions ($^{87}Sr/^{86}Sr(i)$ = 0.7054–0.7065, $\varepsilon_{Nd}(t)$ = −0.6 to +0.3, $\varepsilon_{Hf}(t)$ = +7.39), similar to those of the Duolong andesitic rocks but markedly different from those of the Jurassic Rena Co adakitic granodiorites (Fig. 5a, b). Also, they plot above the terrestrial array, with $\Delta\varepsilon_{Hf}(t)$ = 7.5 (Fig. 5b), resembling the Cretaceous Duolong igneous rocks.

5. Discussion

5.1. Coupling between Nd and Hf isotopes in late Jurassic igneous rocks derived from ancient crust

In Section 4.1, we presented new whole-rock Hf isotope data for the late Jurassic Jiacuo granodiorites and Rena Co adakitic granodiorites. These new data, combined with previous whole-rock Nd isotopes (Supplementary Table 2; Hao et al., 2016a; Sun et al., 2020), reveal Nd–Hf isotopic coupling ($\Delta\varepsilon_{Hf}(t)$ = 0.9 to 2.4) of these Jurassic granodiorites (Fig. 5a).

The Jiacuo granodiorites, which are metaluminous, calc-alkaline, and I-type, have moderate SiO_2 (64.8–68.4 wt%), high K_2O (4.2–5.2 wt%), and low MgO (1.6–2.3 wt%) and Mg# (47–49). These geochemical features are similar to those of lower-crust-derived felsic melts (Li et al., 2014b; Hao et al., 2016a; Wu et al., 2016). Given their enriched isotopic compositions ($^{87}Sr/^{86}Sr(i)$ = 0.7079 to 0.7080, $\varepsilon_{Nd}(t)$ = −7.9 to −7.6), Sun et al. (2020) proposed that the Jiacuo granodiorites were generated by partial melting of SQB ancient mafic lower crust. The Rena Co adakitic granodiorites show high SiO_2 (63.3–66.2 wt%) and K_2O (2.7–3.5 wt%) and low MgO (1.0–1.6 wt%) and Mg# (33–42). The high $(La/Yb)_n$ (23–96) and Sr/Y (51–137) ratios indicate their adakitic affinities. On the basis of the low MgO contents and enriched isotopic compositions, which are similar to those of ancient-lower-crust-derived
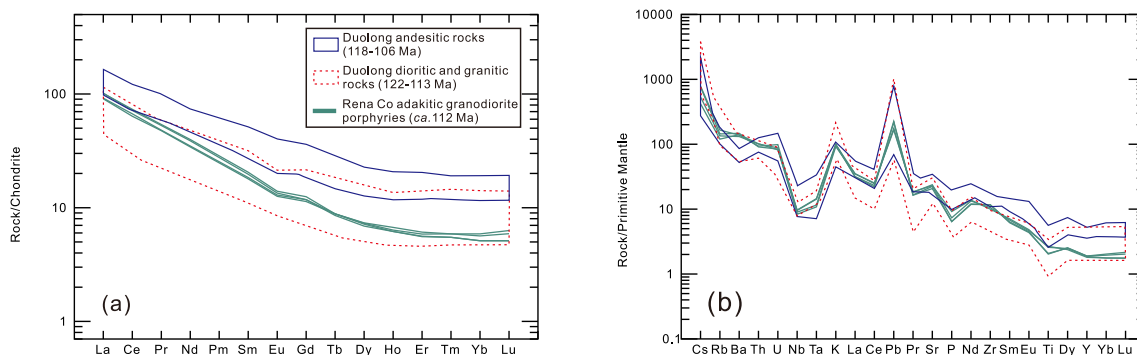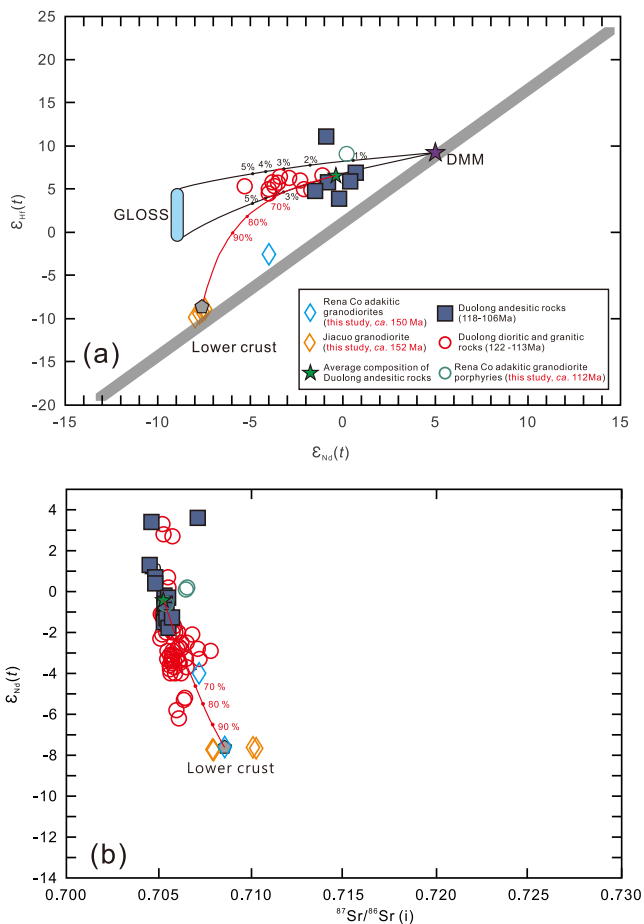

Fig. 4. (a) Chondrite-normalized REE pattern diagram and (b) primitive mantle-normalized trace-element diagram for the SQB early Cretaceous igneous rocks. Data sources are the same as Fig. 2. Chondrite- and primitive-mantle normalization values are from Sun and McDonough (1989).

Fig. 5. (a) $\varepsilon_{Nd}(t)$–$\varepsilon_{Hf}(t)$ diagram for the SQB early Cretaceous igneous rocks. The terrestrial array is after Vervoot et al. (2011) ($\varepsilon_{Hf}(t) = 1.55 \times \varepsilon_{Nd}(t) + 1.21$). The Nd and Hf contents of depleted MORB mantle (DMM), global subducted sediment (GLOSS), and lower crust are from Workman and Hart (2005), Plank (2014), and Rudnick and Gao (2014), respectively. The Nd and Hf isotopic compositions of DMM, GLOSS ($\varepsilon Nd = -8.9$, $\varepsilon Hf = +2 \pm 3$), and lower crust are from Li et al. (2016c), Chauvel et al. (2008), and Hao et al. (2016a), respectively. The residual assemblages in equilibrium with lower-crust-derived melts are assumed to comprise Cpx (40%) + Opx (20%) + Pl (20%) + Amph (19%) + Zircon (1%). The residual mineral assemblage for lower-crust melting is from Qian and Hermann (2013), and the weight fractions of minerals are from Ma et al. (2015). The bulk distribution coefficient (KD) values are from Bédard (2006). (b) $\varepsilon_{Nd}(t)$–$^{87}Sr/^{86}Sr(i)$ diagram for the SQB late Jurassic and early Cretaceous igneous rocks.

magmatic rocks in the SQB, Hao et al. (2016a) suggested that the Rena Co adakitic granodiorites were generated by partial melting of thickened ancient lower crust. In summary, both the Jiacuo granodiorites and Rena Co adakitic granodiorites were likely derived from SQB ancient lower crust and exhibit Nd–Hf isotopic coupling.

5.2. Decoupling of Nd and Hf isotopes in early Cretaceous granitic rocks derived from juvenile crust

Our new data include whole-rock Hf isotopic data of the Rena Co adakitic granodiorite porphyries (*ca.* 112 Ma). These data, combined with existing Nd isotopic data (Hao et al., 2016a), reveal clear Nd–Hf isotopic decoupling ($\Delta\varepsilon_{Hf}(t) = 7.5$; Fig. 5a).

Adakitic rocks are commonly generated by crustal assimilation and high- or low-pressure fractional crystallization (AFC; Castillo et al., 1999; Macpherson et al., 2006), or by partial melting of metabasic rocks (e.g., subducted oceanic crust or subducted, delaminated, or thickened continental lower crust) at eclogite- to amphibolite-facies conditions

(Defant and Drummond, 1990; Atherton and Petford, 1993; Rapp et al., 1999; Chung et al., 2003; Wang et al., 2005). The Rena Co adakitic granodiorite porphyries were not formed by AFC processes from basaltic magmas. La/Y ratios increase in response to high-pressure garnet crystallization, and Mg# values and Cr and Ni contents decrease during low-pressure crystallization of olivine and pyroxene. However, there are no such correlations between SiO_2 and La/Y or Mg# in these adakitic rocks. Besides, their Sr–Nd isotopic compositions ($^{87}Sr/^{86}Sr(i) = 0.7054$–$0.7065$; $\varepsilon_{Nd}(t) = -0.6$ to 0.3) are quite different from those of oceanic-slab-derived adakites of the SQB ($^{87}Sr/^{86}Sr(i) = 0.7043$–$0.7046$; $\varepsilon_{Nd}(t) = 1.0$–$3.4$; Li et al., 2016c), precluding their derivation by partial melting of subducted oceanic crust. In addition, their low MgO (0.4–1.6 wt%) and Mg# (15–42) are inconsistent with derivation from subducted or delaminated continental lower crust, which typically produces adakites with high MgO and Mg# (Xu et al., 2002; Wang et al., 2006). Furthermore, the slightly depleted Sr–Nd isotopes are inconsistent with their origination from ancient lower crust. Therefore, we argue that the early Cretaceous Rena Co adakitic rocks were derived from juvenile lower crust (Hao et al., 2016a).

In summary, our data show that the early Cretaceous Rena Co granitic rocks of the SQB were derived from juvenile lower crust and exhibit Nd–Hf isotopic decoupling. However, the formation and compositions (andesitic or basaltic) of the juvenile lower crust and its role in Nd–Hf isotopic decoupling remain unclear.

5.3. Contribution of mélange melting to the Nd–Hf isotopic decoupling of juvenile crust

Juvenile crust generally has andesitic or basaltic compositions. As only rare basaltic rocks were formed in the SQB during the early Cretaceous, we infer that the early Cretaceous juvenile crust of the SQB was compositionally andesitic. Hao et al. (2016b) suggested that the Cretaceous Duolong andesitic rocks could be a proxy for the juvenile crust of the SQB. Moreover, andesitic juvenile crust is a plausible source of the early Cretaceous felsic rocks (e.g., Rena Co adakitic granodiorite porphyries), for the following reasons: (1) The Sr–Nd isotopic compositions of the juvenile crust are similar to those of the Rena Co adakitic granodiorite porphyries (Fig. 5b); (2) although the Rb/Sr ratios of the Rena Co porphyries are substantially higher than those of juvenile crust, the Rb/Sr ratios of their source rocks, calculated using the methods of Dhuime et al. (2015), are almost identical to those of juvenile crust (Hao et al., 2016b); and (3) the juvenile crust (i.e., the early Cretaceous Duolong andesitic rocks) exhibits strong Nd–Hf isotopic decoupling ($\Delta\varepsilon_{Hf}(t) = 3.0$–$10.3$; Fig. 5a; Supplementary Table 1), consistent with that of the early Cretaceous Rena Co adakitic rocks. Thus, we infer that the early Cretaceous juvenile crust of the SQB was andesitic and was characterized by Nd–Hf isotopic decoupling.

However, the mechanisms that produced the andesitic crust and Nd–Hf isotopic decoupling remain unclear, meaning that it is necessary to investigate the genesis of the Duolong andesitic rocks. Andesitic rocks can be generated by mixing between felsic and mafic magmas, or by AFC from basaltic magmas (e.g., Chen et al., 2014). However, here we suggest that the Duolong andesitic rocks were not formed by these processes, on the basis of the following reasons: (1) In the La–(La/Yb) diagram (Fig. 7c), the samples plot on a partial melting path rather than a fractional crystallization path; and (2) there are no correlations between SiO_2 contents and $\varepsilon_{Nd}(t)$ or $^{87}Sr/^{86}Sr(i)$ values for these rocks (Fig. 7a, b). Rather, the Duolong andesitic rocks are inferred to have been generated by partial melting of a particular source. The source is unlikely to have been the mafic lower crust, as experimental studies have shown that partial melts of basaltic rocks generally have low Mg# (<41), regardless of the degree of melting (e.g., Rapp and Watson, 1995). In contrast, most samples of the Duolong andesitic rocks have high MgO (>3 wt%) and Mg# (>45; Fig. 7d). In fact, the most mafic sample of the Duolong rocks exhibits a low SiO_2 content of 49.4 wt%, which is unlikely to have been derived from mafic lower crust of the
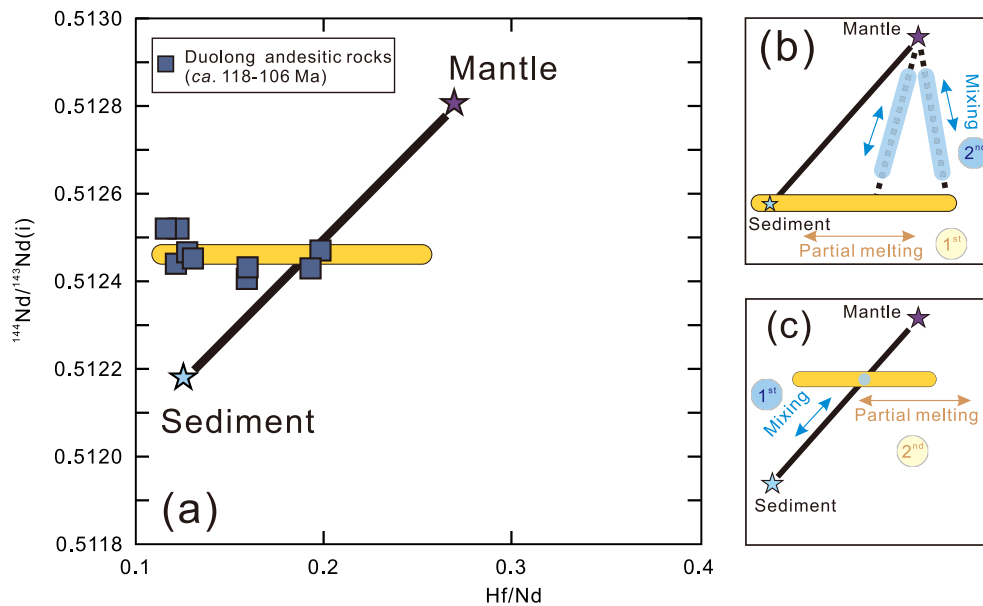
Fig. 6. (a) Nd isotopic compositions versus Hf/Nd ratios for the Cretaceous Duolong andesitic rocks. Mixing lines between the mantle and bulk sediments (bold lines) are presented. (b–c) Trends expected for sediment melting followed by mixing with mantle wedge and for mélange formation followed by melting, respectively, modified from Nielsen and Marschall (2017).
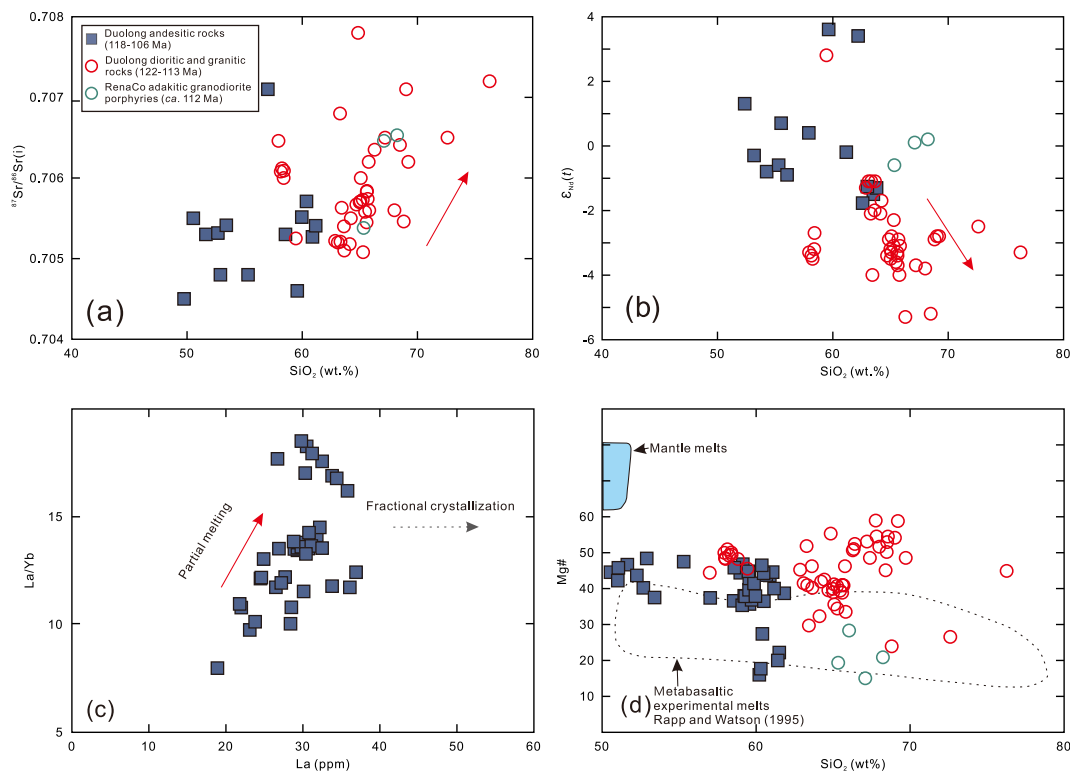
Fig. 7. (a–b) Sr and Nd isotopic compositions versus SiO_2 for the SQB early Cretaceous igneous rocks. (c) (La/Yb)–La diagram for the Cretaceous Duolong andesitic rocks. (d) SiO_2–Mg# diagram for the SQB early Cretaceous igneous rocks. Metabasaltic experimental melt data are from Rapp and Watson (1995).

SQB. Thus, we infer that the Duolong andesitic rocks could have been derived from mafic–ultramafic mantle lithologies. The Duolong andesitic rocks have lower Mg, Cr, and Ni contents and more enriched Sr–Nd–Hf isotopic compositions relative to mid-ocean ridge basalts from typical asthenospheric mantle, indicating a metasomatized mantle source. Subducted sediments probably made a significant contribution to the formation of the Duolong andesitic rocks, according to the following reasons: (1) The early Cretaceous Duolong andesitic rocks

have high $(La/Sm)_N$ ratios and low Ba/Th values (Fig. 8), which is thought to reflect the involvement of subducted sediments (Chen et al., 2014; Hao et al., 2016b); and (2) they show variable (depleted to slightly enriched) Nd–Hf isotopic compositions and plot on the mixing line between depleted mantle and oceanic sediments (Fig. 5a).

Both models discussed above in Section 1 could incorporate subducted sediments into the source of arc magmas. The critical difference between the two models is the order of mixing and trace-element
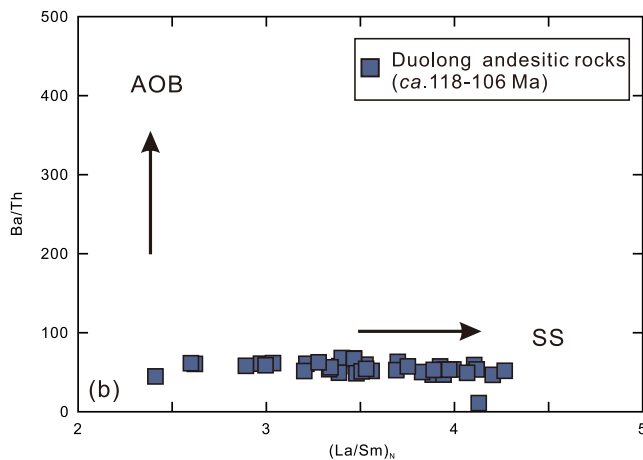
Fig. 8. (Ba/Th)–(La/Sm)$_N$ diagram for the Cretaceous Duolong andesitic rocks. AOB = altered oceanic basalt; SS = seafloor sediments.

fractionation, which could lead to different isotopic mixing relationships (Nielsen and Marschall, 2017). Thus, the (^{144}Nd/^{143}Nd)–(Hf/Nd) diagram (Fig. 6a) should allow these two models to be distinguished (Nielsen and Marschall, 2017). In the conventional model (McCulloch and Gamble, 1991; Elliott et al., 1997), sediment-derived melts mix with the mantle, which should produce a sloping trend (Fig. 6b). In the mélange melting model (Castro et al., 2010, 2013; Marschall and Schumacher, 2012; Nielsen and Marschall, 2017), physical mixing between sediments and the mantle should produce a mélange with relatively homogeneous isotopic compositions, and subsequent partial melting of the mélange should produce an approximately horizontal trend (Fig. 6c). The Duolong andesitic rocks are distributed along a horizontal line (Fig. 6a), indicating that subducted sediments recycled into mantle wedge acted as bulk sediment rather than melts or fluids. Previous studies have concluded that partial melting of the mélange would produce arc magmas dominated by andesitic compositions (e.g., SiO$_2$ = 51–61 wt%; MgO = 1.1–5.7 wt%; Codillo et al., 2018; Cruz-Uribe et al., 2018). The Duolong andesitic rocks have contents of SiO$_2$ (49–62 wt%) and MgO (0.5–6.6 wt%) that are similar to those of mélange-derived melts. Therefore, we suggest that the Duolong andesitic rocks and early Cretaceous andesitic juvenile crust were formed by partial melting of the mélange. The mixing model indicates that the mélange contains 1–2% bulk subducted sediment (Fig. 5a).

This mélange melting model differs from previous interpretations of the petrogenesis of the Duolong andesitic rocks. Li et al. (2016b) suggested that these rocks were derived from a metasomatized mantle wedge with MASH (melting, assimilation, storage and homogenization) processes taking place at the base of the lower crust. However, we propose that the Duolong andesitic rocks were not formed by mixing between felsic and mafic magmas or AFC processes, as discussed above. Wei et al. (2017) suggested that these andesitic rocks may have been derived from a mantle enriched by slab-released fluids. Experimental studies have shown that partial melting of hydrous mantle peridotites usually produces basaltic rocks or high-Mg andesites under particular pressures and temperatures (Blatter and Carmichael, 2001). However, this is not the case for the Duolong andesitic rocks. In the mélange model, andesitic magmas with moderate MgO contents can be directly produced by mélange melting without magma mixing or AFC process, as indicated by experimental studies (Codillo et al., 2018; Cruz-Uribe et al., 2018).

Previous studies have proposed several key mechanisms that can lead to Nd–Hf isotopic decoupling of magmatic rocks: (1) Lower crust that has undergone an ancient anatexis event with residual phases of garnet and zircon may be an optional reservoir for Nd–Hf isotopic decoupling. For example, Schmitz et al. (2004) suggested that residual phases of garnet and zircon changed the Lu/Hf ratios of crustal

protoliths during anatexis. Such ancient anatexis events followed by isotopic evolution are inferred to have caused Nd–Hf isotopic decoupling of the granulitic lower crust beneath southern Africa. (2) Deeply subducted oceanic basalt may serve as the reservoir of Nd–Hf isotopic decoupling. Nowell et al. (2004) argued that Lu/Hf and Sm/Nd behave discordantly in an oceanic crust produced by melting in the garnet stability field. After isotopic evolution for >1 Gyr, this oceanic crust is capable of generating Nd–Hf isotopic decoupling. (3) A magma source involving sediments may show Nd–Hf isotopic decoupling. Partial melting of the mantle wedge metasomatized by slab-released melts (Guo et al., 2014) or mixed with bulk subducted sediment (Marini et al., 2005), could generate magmas with Nd–Hf isotopic decoupling because subducted sediments, as well as their melts, have chemical and isotopic compositions that are distinct from those of mantle ultramafic rocks (Plank and Langmuir, 1998; Chauvel et al., 2008; Yogodzinski et al., 2010).

As demonstrated above, the early Cretaceous granitic rocks (i.e., the Rena Co adakitic granodiorite porphyries) are characterized by Nd–Hf isotopic decoupling. These rocks were derived by partial melting of newly formed lower crust (Hao et al., 2016a). Thus, their Nd–Hf isotopic decoupling could not have been induced by partial melting of ancient lower crust or deeply subducted oceanic crust. Instead, the Nd–Hf isotopic decoupling of the Cretaceous Rena Co adakitic rocks was likely to have been inherited from their juvenile crust source. The juvenile andesitic crust, compositionally represented by the Duolong andesitic rocks, was formed by partial melting of the mélange (a physical mixture of mantle wedge peridotite, altered oceanic basaltic crust, and subducted sediments). Previous work has shown that subducted sediments could have caused Nd–Hf isotopic decoupling in some Cenozoic intraoceanic arc volcanic rocks (Marini et al., 2005; Chauvel et al., 2008, 2009; Yogodzinski et al., 2010; Nebel et al., 2011). Zircons have high Hf contents relative to Lu and other REEs, so the removal or addition of zircons by sedimentary processes is likely to cause fractionation between Nd and Hf in sediments. The incorporation of zircon-free oceanic sediments should change the Nd–Hf isotopic compositions of a mantle source and make the arc magmatic rocks plot above the terrestrial array (Chauvel et al., 2008; Marini et al., 2005). Therefore, we suggest that the Nd–Hf isotopic decoupling of the early Cretaceous granitic and andesitic rocks in the SQB reflects the mélange contribution to arc magmas.

5.4. A test of our model

Our model posits that the SQB early Cretaceous andesitic juvenile crust was characterized by Nd–Hf isotopic decoupling. Thus, the early Cretaceous intermediate–felsic rocks in the SQB that are genetically linked to andesitic rocks should also show Nd–Hf isotopic decoupling. For this reason, the early Cretaceous Duolong dioritic and granitic rocks provide a test for our model.

The variable Sr–Nd isotopic compositions of the Duolong dioritic and granitic rocks overlap those of the Duolong andesitic rocks. In addition, these two types of rocks (dioritic–granitic and andesitic) show close temporal–spatial correlations. Thus, we infer that the Duolong dioritic and granitic rocks are genetically linked to the Duolong andesitic rocks. The former show lower REE contents than the latter, indicating that the former cannot have been formed by FC processes of the mélange-derived Duolong andesitic magmas. We instead interpret that the Duolong dioritic and granitic rocks were likely formed by mixing of such andesitic melts and ancient-lower-crust-derived magmas, on the basis of the following reasons: (1) The ε$_{Nd}$(t) and ^{87}Sr/^{86}Sr(i) values of these rocks are correlated with SiO$_2$ content, consistent with magma mixing (Fig. 7a, b); and (2) these rocks plot on a mixing trend between an end-member isotopically similar to the Duolong andesitic rocks and an end-member similar to ancient lower crust of the SQB (Fig. 5b). The mixing modeling (Fig. 7a, b) indicates that mixing of 0–70% ancient-lower-crust-derived melts and mélange-derived andesitic melts can produce the Duolong intermediate–felsic intrusive rocks.

The early Cretaceous Duolong dioritic and granitic rocks show strong Nd–Hf isotopic decoupling ($\Delta\varepsilon_{Hf}(t) = 6.3$–$10.0$; Fig. 5a; Supplementary Table 1), similar to that of the Duolong andesitic rocks. Combining this information with that for the early Cretaceous Rena Co adakitic rocks, we suggest that the mélange melting contributed to the generation of the SQB early Cretaceous andesitic juvenile crust, which was characterized by Nd–Hf isotopic decoupling (i.e., the Duolong andesitic rocks), and that the andesitic material contributed to the formation of the early Cretaceous intermediate–felsic rocks in the SQB, which also show Nd–Hf isotopic decoupling (e.g., the Duolong dioritic and granitic rocks and Rena Co adakitic rocks).

5.5. Geodynamics of the southern Qiangtang Block during the late Mesozoic

The tectonic setting of the SQB during the late Mesozoic is still disputed. However, there is increasing evidence to indicate that the BNTO survived until the late early Cretaceous (*ca.* 100 Ma). Magmatic rocks diagnostic of oceanic subduction have been identified in the SQB

(e.g., 110–104 Ma adakites and Nb-enriched basalts; Hao et al., 2019). In addition, numerous early Cretaceous oceanic basalts within the BNSZ reflect survival of the BNTO until at least the late early Cretaceous (*ca.* 100 Ma; Bao et al., 2007; Zhang et al., 2012, 2014; Wang et al., 2016). Therefore, we infer that the SQB was in a continental margin arc setting during the late Mesozoic and that the BNTO did not close until the late early Cretaceous (*ca.* 100 Ma; Zhang et al., 2012). In this case, the magmatic gap from *ca.* 148 to 122 Ma in the SQB can be explained by flat subduction of the BNTO slab owing to oceanic plateau subduction (Hao et al., 2019).

In summary, the late Mesozoic tectono-magmatic evolution of the SQB can be described as follows (Fig. 9): (1) During the late Jurassic (169–148 Ma), normal northward subduction of the BNTO slab induced partial melting of ancient lower crust, which generated the SQB Jurassic felsic magmatism with Nd–Hf isotopic coupling (e.g., in the Jiacuo and Rena Co areas). (2) Continental arc magmatism ceased as a result of flat subduction of the BNTO slab during the early Cretaceous (148–122 Ma). Notably, substantial volumes of mélange rocks were able to form in the subduction channel during this period (Hao et al., 2016b, 2019). (3)
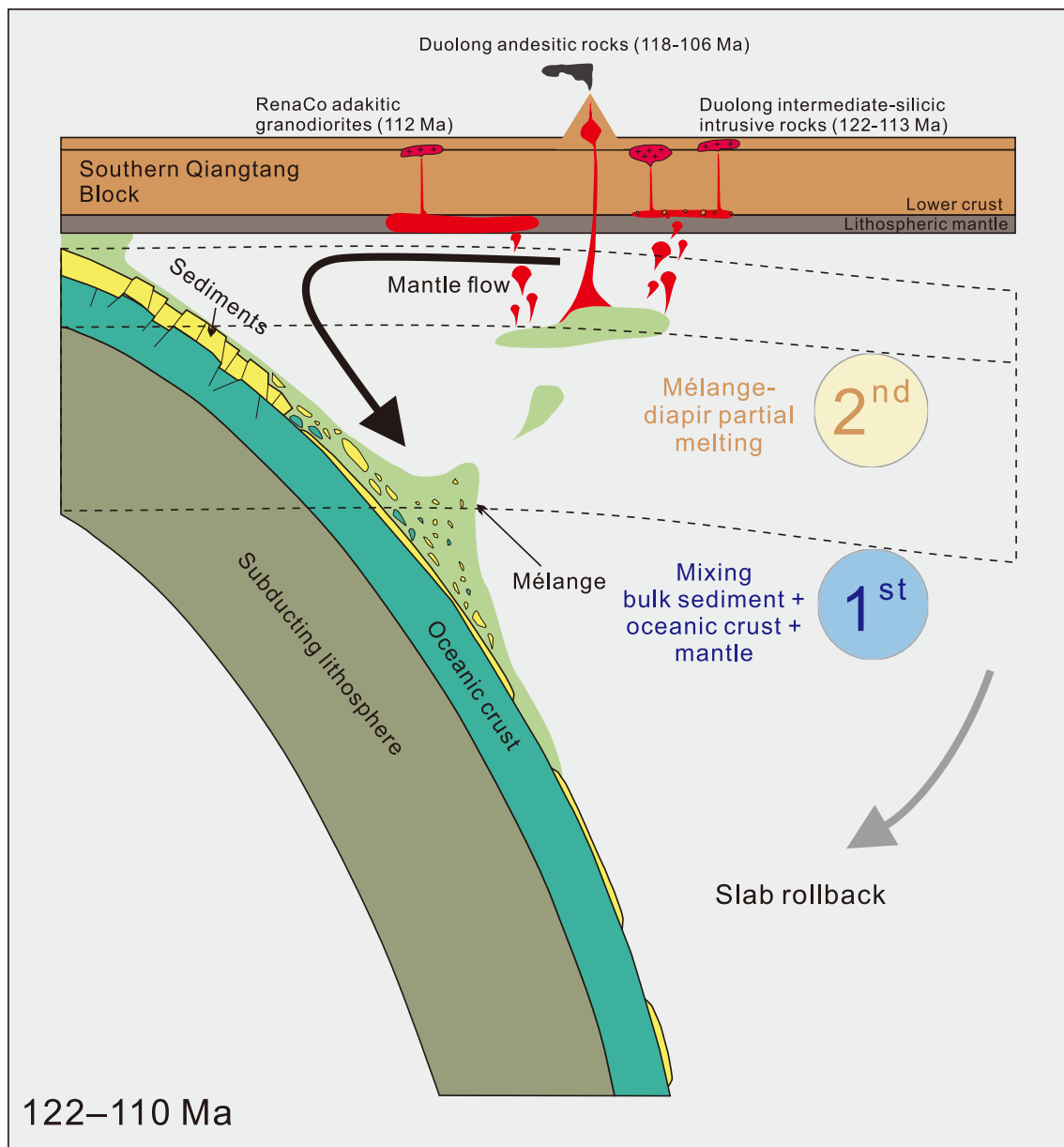

Fig. 9. A conceptual model illustrating the tectono-magmatic evolution of central Tibet during the late Mesozoic (not to scale). See the text in Section 5.5 for details.

Rollback of the BNTO slab from 122 Ma induced upwelling of the asthenospheric mantle and partial melting of the mélange. Primary andesitic melts derived from the mélange were erupted to form the Duolong andesitic rocks (118–106 Ma). Mixing between the andesitic melts and ancient-lower-crust-derived magmas formed the Duolong dioritic and granitic rocks (122–113 Ma). In addition, the primary andesitic melts underplated the SQB lower crust to form relatively juvenile andesitic crust. Partial melting of this thickened juvenile andesitic lower crust formed the Rena Co adakitic granodiorites (112 Ma). The early Cretaceous andesitic–felsic rocks show Nd–Hf isotopic decoupling, which is ascribed to the incorporation of partial melts of the mélange.

6. Conclusions

(1) The late Jurassic igneous rocks of the SQB were generated by partial melting of ancient lower crust and show Nd–Hf isotopic coupling. Conversely, the early Cretaceous igneous rocks of the SQB were produced by partial melting of juvenile crust and show marked Nd–Hf isotopic decoupling.

(2) The early Cretaceous juvenile crust of the SQB was andesitic and exhibited Nd–Hf isotopic decoupling, and was generated by partial melting of the subduction mélange.

(3) Flat subduction and subsequent rollback of the BNTO slab caused the formation and partial melting of the mélange, respectively.

CRediT authorship contribution statement

Peng Sun: Conceptualization, Formal analysis, Writing – original draft, Visualization. **Qiang Wang:** Conceptualization, Writing – review & editing, Supervision, Project administration. **Lu-Lu Hao:** Investigation, Writing – review & editing, Project administration. **Wei Dan:** Investigation, Writing – review & editing. **Quan Ou:** Writing – review & editing. **Zi-Qi Jiang:** Investigation. **Gong-Jian Tang:** Writing – review & editing.

Declaration of Competing Interest

The authors declare that they have no known competing financial interests or personal relationships that could have appeared to influence the work reported in this paper.

Appendix A. Supplementary material

Supplementary data to this article can be found online at https://doi. org/10.1016/j.jseaes.2021.104931.

References

Atherton, M.P., Petford, N., 1993. Generation of sodium-rich magmas from newly underplated basaltic crust. Nature 362 (6416), 144–146.

Bao, P.S., Xiao, X.C., Su, L., Wang, J., 2007. Petrological, geochemical and chronological constraints for the tectonic setting of the Dongco ophiolite in Tibet. Sci. China, Ser. D Earth Sci. 50 (5), 660–671.

Barry, T.L., Pearce, J.A., Leat, P.T., Millar, I.L., le Roex, A.P., 2006. Hf isotope evidence for selective mobility of high-field-strength elements in a subduction setting: south sandwich islands. Earth Planet. Sci. Lett. 252 (3-4), 223–244.

Bédard, J.H., 2006. A catalytic delamination-driven model for coupled genesis of archaean crust and sub-continental lithospheric mantle. Geochim. Cosmochim. Acta 70 (5), 1188–1214.

Blatter, D.L., Carmichael, I.S.E., 2001. Hydrous phase equilibria of a mexican high-silica andesite: a candidate for a mantle origin? Geochim. Cosmochim. Acta 65 (21), 4043–4065.

Cao, Y., Sun, Z., Li, H., Ye, X., Pan, J., Liu, D., Zhang, L., Wu, B., Cao, X., Liu, C., Yang, Z., 2020. Paleomagnetism and U-Pb geochronology of early cretaceous volcanic rocks from the Qiangtang block, Tibetan Plateau: implications for the Qiangtang-Lhasa collision. Tectonophysics 789, 228500. https://doi.org/10.1016/j.tecto.2020.228500.

Castillo, P.R., Janney, P.E., Solidum, R.U., 1999. Petrology and geochemistry of camiguin island, southern Philippines: insights to the source of adakites and other lavas in a complex arc setting. Contrib. Mineral. Petrol. 134 (1), 33–51.

Castro, A., Gerya, T., García-Casco, A., Fernández, C., Díaz-Alvarado, J., Moreno-Ventas, I., Löw, I., 2010. Melting relations of morb-sediment mélanges in underplated mantle wedge plumes: implications for the origin of cordilleran-type batholiths. J. Petrol. 51, 1267–1295.

Castro, A., Vogt, K., Gerya, T., 2013. Generation of new continental crust by sublithospheric silicic-magma relamination in arcs: a test of Taylor's andesite model. Gondwana Res. 23 (4), 1554–1566.

Chauvel, C., Lewin, E., Carpentier, M., Arndt, N.T., Marini, J.C., 2008. Role of recycled oceanic basalt and sediment in generating the Nd-Hf mantle array. Nat. Geosci. 1, 64.

Chauvel, C., Marini, J.C., Plank, T., Ludden, J.N., 2009. Hf-Nd input flux in the izu-mariana subduction zone and recycling of subducted material in the mantle. Geochem. Geosys. Geosyst. 10.

Chen, L., Zhao, Z.F., Zheng, Y.F., 2014. Origin of andesitic rocks: geochemical constraints from mesozoic volcanics in the Luzong Basin, South China. Lithos 190-191, 220–239.

Chung, S.L., Chu, M.F., Zhang, Y.Q., Xie, Y.W., Lo, C.H., Lee, T.Y., Lan, C.Y., Li, X.H., Zhang, Q., Wang, Y.Z., 2005. Tibetan tectonic evolution inferred from spatial and temporal variations in post-collisional magmatism. Earth Sci. Rev. 68, 173–196.

Chung, S.L., Liu, D.Y., Ji, J.Q., Chu, M.F., Lee, H.Y., Wen, D.J., Lo, C.H., Lee, T.Y., Qian, Q., Zhang, Q., 2003. Adakites from continental collision zones: melting of thickened lower crust beneath Southern Tibet. Geology 31, 1021–1024.

Codillo, E.A., Le Roux, V., Marschall, H.R., 2018. Arc-like magmas generated by mélange-peridotite interaction in the mantle wedge. Nat. Commun. 9, 1–11.

Cruz-Uribe, A.M., Marschall, H.R., Gaetani, G.A., Le Roux, V., 2018. Generation of alkaline magmas in subduction zones by partial melting of mélange diapirs—an experimental study. Geology 46, 343–346.

Defant, M.J., Drummond, M.S., 1990. Derivation of some modern arc magmas by melting of young subducted lithosphere. Nature 347 (6294), 662–665.

Dhuime, B., Wuestefeld, A., Hawkesworth, C.J., 2015. Emergence of modern continental crust about 3 billion years ago. Nat. Geosci. 8 (7), 552–555.

Elliott, T., Plank, T., Zindler, A., White, W., Bourdon, B., 1997. Element transport from slab to volcanic front at the mariana arc. J. Geophys. Res. Solid Earth 102, 14991–15019.

Fan, J.J., Li, C., Xie, C.M., Wang, M., Chen, J.W., 2015. Petrology and U-Pb zircon geochronology of bimodal volcanic rocks from the maierze group, northern tibet: constraints on the timing of closure of the Banggong-Nujiang Ocean. Lithos 227, 148–160.

Guo, F., Fan, W., Li, C., Wang, C.Y., Li, H., Zhao, L., Li, J., 2014. Hf–Nd–O isotopic evidence for melting of recycled sediments beneath the Sulu Orogen, North China. Chem. Geol. 381, 243–258.

Hao, L.L., Wang, Q., Wyman, D.A., Ou, Q., Dan, W., Jiang, Z.Q., Wu, F.Y., Yang, J.H., Long, X.P., Li, J., 2016a. Underplating of basaltic magmas and crustal growth in a continental arc: evidence from late mesozoic intermediate-felsic intrusive rocks in Southern Qiangtang, Central Tibet. Lithos 245, 223–242.

Hao, L.L., Wang, Q., Wyman, D.A., Ou, Q., Dan, W., Jiang, Z.Q., Yang, J.H., Li, J., Long, X.P., 2016b. Andesitic crustal growth via mélange partial melting: evidence from early cretaceous arc dioritic/andesitic rocks in Southern Qiangtang, Central Tibet. Geochem. Geophys. Geosyst. 17 (5), 1641–1659.

Hao, L.L., Wang, Q., Zhang, C.F., Ou, Q., Yang, J.H., Dan, W., Jiang, Z.Q., 2019. Oceanic plateau subduction during closure of the Bangong-Nujiang Tethyan Ocean: insights from central tibetan volcanic rocks. Geol. Soc. Am. Bull. 131, 864–880.

Hawkesworth, C., Turner, S., Peate, D., McDermott, F., van Calsteren, P., 1997. Elemental U and Th variations in island arc rocks: implications for U-series isotopes. Chem. Geol. 139 (1-4), 207–221.

Kapp, P., Murphy, M.A., Yin, A., Harrison, T.M., Ding, L., Guo, J.H., 2003. Mesozoic and cenozoic tectonic evolution of the shiquanhe area of Western Tibet. Tectonics 22.

Li, G.M., Qin, K.Z., Li, J.X., Evans, N.J., Zhao, J.X., Cao, M.J., Zhang, X.N., 2017a. Cretaceous magmatism and metallogeny in the Bangong-Nujiang Metallogenic Belt, Central Tibet: evidence from petrogeochemistry, zircon U-Pb Ages, and Hf-O isotopic compositions. Gondwana Res. 41, 110–127.

Li, J.X., Qin, K.Z., Li, G.M., Evans, N.J., Zhao, J.X., Cao, M.J., Huang, F., 2016a. The nadun Cu–Au mineralization, Central Tibet: root of a high sulfidation epithermal deposit. Ore Geol. Rev. 78, 371–387.

Li, J.X., Qin, K.Z., Li, G.M., Richards, J.P., Zhao, J.X., Cao, M.J., 2014a. Geochronology, geochemistry, and zircon Hf isotopic compositions of mesozoic intermediate-felsic intrusions in Central Tibet: petrogenetic and tectonic implications. Lithos 198-199, 77–91.

Li, J.X., Qin, K.Z., Li, G.M., Xiao, B.o., Zhao, J.X., Cao, M.J., Chen, L., 2013. Petrogenesis of ore-bearing porphyries from the duolong porphyry Cu-Au deposit, Central Tibet: evidence from U-Pb geochronology, petrochemistry and Sr-Nd-Hf-O isotope characteristics. Lithos 160-161, 216–227.

Li, J.X., Qin, K.Z., Li, G.M, Xiao, B., Zhao, J.X., Chen, L., 2011. Magmatic-hydrothermal evolution of the cretaceous duolong gold-rich porphyry copper deposit in the Bangongco Metallogenic Belt, Tibet: evidence from U-Pb and ^{40}Ar/^{39}Ar geochronology. J. Asian Earth Sci. 41 (6), 525–536.

Li, J.X., Qin, K.Z., Li, G.M., Xiao, B.O., Zhao, J.X., Chen, L., 2016b. Petrogenesis of cretaceous igneous rocks from the duolong porphyry Cu-Au deposit, Central Tibet: evidence from zircon U-Pb geochronology, petrochemistry and Sr-Nd-Pb-Hf isotope characteristics. Geol. J. 51 (2), 285–307.

Li, S., Yin, C., Guilmette, C., Ding, L., Zhang, J., 2019. Birth and demise of the bangong-nujiang tethyan ocean: a review from the Gerze Area of Central Tibet. Earth Sci. Rev. 198, 102907. https://doi.org/10.1016/j.earscirev.2019.102907.

Li, S.M., Zhu, D.C., Wang, Q., Zhao, Z., Zhang, L.L., Liu, S.A., Chang, Q.S., Lu, Y.H., Dai, J.G., Zheng, Y.C., 2016c. Slab-derived adakites and subslab asthenosphere-derived OIB-type rocks at 156 ± 2 Ma from the North of Gerze, Central Tibet: records of the Bangong-Nujiang oceanic ridge subduction during the late jurassic. Lithos 262, 456–469.

Li, S.M., Zhu, D.C., Wang, Q., Zhao, Z.D., Sui, Q.L., Liu, S.A., Liu, D., Mo, X.X., 2014b. Northward subduction of Bangong-Nujiang Tethys: insight from late jurassic intrusive rocks from Bangong Tso in Western Tibet. Lithos 205, 284–297.

Li, X.H., Li, Z.X., Wingate, M.T.D., Chung, S.L., Liu, Y., Lin, G.C., Li, W.X., 2006. Geochemistry of the 755 Ma Mundine Well dyke swarm, northwestern Australia: Part of a Neoproterozoic mantle superplume beneath Rodinia? Precambr. Res. 146 (1–2), 1–15.

Li, X.K., Li, C., Sun, Z.M., Wang, M., 2017b. Origin and Tectonic Setting of the Giant Duolong Cu–Au Deposit, South Qiangtang Terrane, Tibet: Evidence from Geochronology and Geochemistry of Early Cretaceous Intrusive Rocks. Ore Geol. Rev. 80, 61–78.

Li, Y., He, J., Han, Z., Wang, C., Ma, P., Zhou, A., Liu, S.A., Xu, M., 2016d. Late Jurassic sodium-rich adakitic intrusive rocks in the southern Qiangtang Terrane, central Tibet, and their implications for the Bangong-Nujiang Ocean subduction. Lithos 245, 34–46.

Liu, D., Huang, Q., Fan, S., Zhang, L., Shi, R., Ding, L., 2014. Subduction of the Bangong-Nujiang Ocean: constraints from granites in the Bangong Co Area, Tibet. Geol. J. 49 (2), 188–206.

Liu, H., Huang, Q., Uysal, I.T., Cai, Z., Wan, Z., Xia, B., Zheng, H., Yang, P., 2020. Geodynamics of the divergent double subduction along the Bangong-Nujiang Tethyan suture zone: Insights from late Mesozoic intermediate-mafic rocks in central Tibet. Gondwana Res. 79, 233–247.

Ma, Q., Zheng, J.P., Xu, Y.G., Griffin, W.L., Zhang, R.S., 2015. Are continental 'adakites' derived from thickened or foundered lower crust? Earth Planet. Sci. Lett. 419, 125–133.

Macpherson, C.G., Dreher, S.T., Thirlwall, M.F., 2006. Adakites without Slab Melting: high pressure differentiation of island Arc Magma, Mindanao, the Philippines. Earth Planet. Sci. Lett. 243 (3-4), 581–593.

Marini, J.C., Chauvel, C., Maury, R.C., 2005. Hf Isotope Compositions of Northern Luzon Arc Lavas Suggest Involvement of Pelagic Sediments in Their Source. Contrib. Mineral. Petrol. 149 (2), 216–232.

Marschall, H.R., Schumacher, J.C., 2012. Arc magmas sourced from mélange diapirs in subduction zones. Nat. Geosci. 5 (12), 862–867.

McCulloch, M.T., Gamble, J.A., 1991. Geochemical and geodynamical constraints on subduction zone magmatism. Earth Planet. Sci. Lett. 102 (3-4), 358–374.

Middlemost, E.A.K., 1994. Naming materials in the magma/igneous rock system. Earth-Sci. Rev. 37 (3-4), 215–224.

Nebel, O., Vroon, P.Z., van Westrenen, W., Iizuka, T., Davies, G.R., 2011. The Effect of sediment recycling in subduction zones on the Hf isotope character of new arc crust, banda arc, Indonesia. Earth Planet. Sci. Lett. 303 (3-4), 240–250.

Nielsen, S.G., Marschall, H.R., 2017. Geochemical evidence for mélange melting in global arcs. Sci. Adv. 3 (4), e1602402. https://doi.org/10.1126/sciadv.1602402.

Nowell, G., Pearson, D., Bell, D., Carlson, R., Smith, C., Kempton, P., Noble, S., 2004. Hf isotope systematics of kimberlites and their megacrysts: new constraints on their source regions. J. Petrol. 45, 1583–1612.

Peccerillo, A., Taylor, S.R., 1976. Geochemistry of eocene calc-alkaline volcanic rocks from the Kastamonu Area, Northern Turkey. Contrib. Mineral. Petrol. 58 (1), 63–81.

Plank, T., 2005. Constraints from thorium/lanthanum on sediment recycling at subduction zones and the evolution of the continents. J. Petrol. 46, 921–944.

Plank, T., 2014. The chemical composition of subducting sediments. Treat. Geochem. 4, 607–629.

Plank, T., Langmuir, C.H., 1993. Tracing trace elements from sediment input to volcanic output at subduction zones. Nature 362 (6422), 739–743.

Plank, T., Langmuir, C.H., 1998. The chemical composition of subducting sediment and its consequences for the crust and mantle. Chem. Geol. 145, 325–394.

Porter, K.A., White, W.M., 2009. Deep mantle subduction flux. Geochem. Geophys. Geosyst. 10.

Qian, Q., Hermann, J., 2013. Partial melting of lower crust at 10–15 kbar: Constraints on adakite and TTG formation. Contrib. Mineral. Petrol. 165, 1195–1224.

Rapp, R.P., Shimizu, N., Norman, M.D., Applegate, G.S., 1999. Reaction between slab-derived melts and peridotite in the mantle wedge: experimental constraints at 3.8 Gpa. Chem. Geol. 160 (4), 335–356.

Rapp, R.P., Watson, E.B., 1995. Dehydration melting of metabasalt at 8–32 Kbar: implications for continental growth and crust-mantle recycling. J. Petrol. 36, 891–931.

Rudnick, R., Gao, S., 2014. Composition of the continental crust. Treat. Geochem. 4, 1–51.

Schmitz, M.D., Vervoort, J.D., Bowring, S.A., Patchett, P.J., 2004. Decoupling of the Lu-Hf and Sm-Nd isotope systems during the evolution of granulitic lower crust beneath Southern Africa. Geology 32 (5), 405. https://doi.org/10.1130/G20241.110.1130/2004067.

Sun, P., Dan, W., Wang, Q., Tang, G.J., Ou, Q., Hao, L.L., Jiang, Z.Q., 2020. Zircon U-Pb geochronology and Sr–Nd–Hf–O isotope geochemistry of Late Jurassic granodiorites in the Southern Qiangtang Block, Tibet: remelting of ancient mafic lower crust in an arc setting? J. Asian Earth Sci. 192, 104235. https://doi.org/10.1016/j.jseaes.2020.104235.

Sun, S.S., McDonough, W.F., 1989. Chemical and isotopic systematics of oceanic basalts: implications for mantle composition and processes. Geological Society, London, Special Publications 42 (1), 313–345.

Vervoort, J.D., Plank, T., Prytulak, J., 2011. The Hf–Nd isotopic composition of marine sediments. Geochim. Cosmochim. Acta 75 (20), 5903–5926.

Wang, B.D., Wang, L.Q., Chung, S.L., Chen, J.L., Yin, F.G., Liu, H., Li, X.B., Chen, L.K., 2016. Evolution of the Bangong-Nujiang Tethyan Ocean: insights from the geochronology and geochemistry of mafic rocks within ophiolites. Lithos 245, 18–33.

Wang, Q., McDermott, F., Xu, J.F., Bellon, H., Zhu, Y.T., 2005. Cenozoic K-rich adakitic volcanic rocks in the Hohxil Area, Northern Tibet: lower-crustal melting in an intracontinental setting. Geology 33 (6), 465. https://doi.org/10.1130/G21522.110.1130/2005088.

Wang, Q., Tang, J.X., Fang, X., Lin, B., Song, Y., Wang, Y.Y., 2015. Petrogenetic Setting of Andesites in Rongna Ore Block, Tiegelong Cu (Au-Ag) Deposit, Duolong Ore Concentration Area, Tibet: Evidence from Zircon U-Pb La-Icp-Ms Dating and Petrogeochemistry of Andesites. Geol. China 42, 1324–1336 (in Chinese with English abstract).

Wang, Q., Xu, J.F., Jian, P., Bao, Z.W., Zhao, Z.H., Li, C.F., Xiong, X.L., Ma, J.L., 2006. Petrogenesis of adakitic porphyries in an extensional tectonic setting, dexing, South China: implications for the genesis of porphyry copper mineralization. J. Petrol. 47, 119–144.

Wei, S.G., Tang, J.X., Song, Y., Liu, Z.b., Feng, J., Li, Y.b., 2017. Early Cretaceous bimodal volcanism in the Duolong Cu Mining District, Western Tibet: record of slab breakoff that triggered ca. 108–113 ma magmatism in the Western Qiangtang Terrane. J. Asian Earth Sci. 138, 588–607.

Workman, R.K., Hart, S.R., 2005. Major and trace element composition of the depleted morb mantle (Dmm). Earth Planet. Sci. Lett. 231 (1-2), 53–72.

Wu, H., Xie, C., Li, C., Wang, M., Fan, J., Xu, W., 2016. Tectonic shortening and crustal thickening in subduction zones: evidence from middle-late jurassic magmatism in Southern Qiangtang, China. Gondwana Res. 39, 1–13.

Xu, J.F., Shinjo, R., Defant, M.J., Wang, Q., Rapp, R.P., 2002. Origin of mesozoic adakitic intrusive rocks in the Ningzhen Area of East China: partial melting of delaminated lower continental crust? Geology 30, 1111–1114.

XZBGM (Xizang Bureau of Geology and Mineral Resources), 1993. Regional Geology of Xizang Autonomous Region, China, with geologic map (1: 1500000). Beijing, Geological Publishing House, 707.

Yang, Z.Y., Wang, Q., Hao, L.L., Wyman, D.A., Ma, L., Wang, J., Qi, Y., Sun, P., Hu, W.L., 2021. Subduction erosion and crustal material recycling indicated by adakites in central Tibet. Geology 49, 708–712.

Yang, Z.Y., Wang, Q., Yang, J.H., Dan, W., Zhang, X.Z., Ma, L., Qi, Y., Wang, J., Sun, P., 2019a. Petrogenesis of Early Cretaceous granites and associated microgranular enclaves in the Xiabie Co area, central Tibet: crust-derived magma mixing and melt extraction. Lithos 350–351, 105199.

Yang, Z.Y., Wang, Q., Zhang, C., Yang, J.H., Ma, L., Wang, J., Sun, P., Qi, Y., 2019b. Cretaceous (~100 Ma) high-silica granites in the Gajin area, Central Tibet: Petrogenesis and implications for collision between the Lhasa and Qiangtang Terranes. Lithos 324–325, 402–417.

Yin, A., Harrison, T.M., 2000. Geologic Evolution of the Himalayan-Tibetan Orogen. Ann. Rev. Earth Planet. Sci. 28, 211–280.

Yogodzinski, G., Vervoort, J., Brown, S.T., Gerseny, M., 2010. Subduction Controls of Hf and Nd Isotopes in Lavas of the Aleutian Island Arc. Earth Planet. Sci. Lett. 300, 226–238.

Zhang, K.J., 2004. Secular geochemical variations of the Lower Cretaceous siliciclastic rocks from central Tibet (China) indicate a tectonic transition from continental collision to back-arc rifting. Earth Planet. Sci. Lett. 229, 73–89.

Zhang, K.J., Tang, X.C., 2009. Eclogites in the interior of the Tibetan Plateau and their geodynamic implications. Chin. Sci. Bull. 54, 2556–2567.

Zhang, K.J., Xia, B., Zhang, Y.X., Liu, W.L., Zeng, L., Li, J.F., Xu, L.F., 2014. Central Tibetan Meso-Tethyan Oceanic Plateau. Lithos 210–211, 278–288.

Zhang, K.J., Zhang, Y.X., Tang, X.C., Xia, B., 2012. Late Mesozoic Tectonic Evolution and Growth of the Tibetan Plateau Prior to the Indo-Asian Collision. Earth Sci. Rev. 114, 236–249.

Zhang, Y.X., Jin, X., Zhang, K.J., Sun, W.D., Liu, J.M., Zhou, X.Y., Yan, L.L., 2018. Newly Discovered Late Triassic Baqing Eclogite in Central Tibet Indicates an Anticlockwise West-East Qiangtang Collision. Sci. Rep. 8, 1–12.

Zhang, Y.X., Li, Z.W., Yang, W.G., Zhu, L.D., Jin, X., Zhou, X.Y., Tao, G., Zhang, K.J., 2017. Late Jurassic-Early Cretaceous Episodic Development of the Bangong Meso-Tethyan Subduction: Evidence from Elemental and Sr–Nd Isotopic Geochemistry of

Arc Magmatic Rocks, Gaize Region, Central Tibet, China. J. Asian Earth Sci. 135, 212–242.

Zhu, D.C., Li, S.M., Cawood, P.A., Wang, Q., Zhao, Z.D., Liu, S.A., Wang, L.Q., 2016. Assembly of the Lhasa and Qiangtang Terranes in Central Tibet by Divergent Double Subduction. Lithos 245, 7–17.

Zhu, X.P., Chen, H.A., Liu, H.F., Ma, D.F., Li, G.M., Huang, H.X., Zhang, H., Liu, C.Q., Wei, L.J., 2015a. Zircon U-Pb Ages, Geochemistry of the Porphyries from the

Duobuza Porphyry Cu-Au Deposit, Tibet and Their Metallogenic Significance. Acta Geol. Sin. 89, 534–548 (in Chinese with English abstract).

Zhu, X.P., Chen, H.A., Liu, H.F., Ma, D.F., Li, G.M., Zhang, H., Liu, C.Q., Wei, L.J., 2015b. Geochronology and Geochemistry of Porphyries from the Naruo Porphyry Copper Deposit, Tibet and Their Metallogenic Significance. Acta Geol. Sin. 89, 109–128 (in Chinese with English abstract).

Zindler, A., Hart, S., 1986. Chemical geodynamics. Ann. Rev. Earth Planet. Sci. 14, 493–571.